Journal of Structural Geology, Vol. 15, No. 2, pp. 163 to 176, 1993
Printed in Great Britain

0191-8141/93 $06.00+0.00

Tectonic evolution of the Bindura–Shamva greenstone belt (northern Zimbabwe): progressive deformation around diapiric batholiths

H. A. JELSMA and P. A. VAN DER BEEK

Institute of Earth Sciences, Vrije Universiteit, De Boelelaan 1085, 1081 HV Amsterdam, The Netherlands

and

M. L. VINYU

Department of Geology, University of Zimbabwe, P.O. Box MP 167, Mt. Pleasant, Harare, Zimbabwe

(*Received* 3 *June* 1991; *accepted in revised form* 12 *July* 1992)

Abstract—The Bindura–Shamva greenstone belt (northern Zimbabwe) and adjacent batholiths are regarded as one of the type areas for granite–greenstone tectonics. Structural observations and three-dimensional strain analyses have been used to propose a model for the tectonic evolution of this late Archaean greenstone belt. The data indicate that pluton emplacement triggered the deformation of the greenstone sequences and that the deformation history is single-phase progressive rather than polyphase. They do not, however, lead to an unambiguous interpretation of the emplacement mechanism. Structural features are best explained by a combination of pluton diapirism and ballooning plutonism. Criteria used as evidence for pluton-related deformation include the pattern of foliation and stretching lineation trajectories, the variation in strain type and strain intensity, fold types, sense of shear at the batholith–greenstone interface, metamorphic zoning and timing of porphyroblast growth. Specific structural and strain patterns within cleavage triple points, interdomal synclinoria (saddle culminations) and batholith margins demonstrate interference between strain fields developed around each batholith.

INTRODUCTION

THE tectonic relationship between Archaean greenstone belts and surrounding batholiths has been a subject of debate for several decades (Macgregor 1951, Anhaeusser *et al.* 1969, Gorman *et al.* 1978, Platt 1980, De Wit & Ashwall 1986). One of the main issues is the relative importance of 'vertical' or 'diapiric' tectonic models vs 'horizontal' crustal shortening models to explain the dome-and-keel configuration of granite–gneiss terrains and enveloping greenstone belts. A dome-and-keel configuration has been attributed to either simultaneous or successive cross-folding, magmatic or solid-state diapirism, ballooning plutonism, or a combination of these processes (e.g. Brun *et al.* 1981, Soula 1982, Dixon & Summers 1983, Bleeker & Westra 1987, Talbot 1987, Veenhof & Stel 1991).

The historical development of different models for the evolution of the Bindura–Shamva greenstone belt may serve as an example of the controversies concerning vertical and horizontal tectonic models. In a classic paper, Macgregor (1951) explained the relationship between batholiths and surrounding greenstone belts in Zimbabwe by polyphase deformation and diapiric intrusion of granitoid batholiths into more dense greenstone sequences (Fig. 1). His 'gregarious' batholith model was adopted by, among others, Anhaeusser *et al.* (1969), Viljoen & Viljoen (1969), Anhaeusser (1973) and Viewing & Harrison (1973). Ramsay (1975, 1989) interpreted the Chinamora batholith as a spherically inflating ('ballooning') pluton at a relatively immature stage of diapirism. In this model, the injection of successive magma pulses of increasingly siliceous composition leads to progressive syn-emplacement expansion of the previously consolidated igneous material, the margin of the batholith and the greenstone envelope.

Snowden & Bickle (1976), Snowden & Snowden (1979) and Snowden (1984), however, proposed that the dome and keel structures resulted from interference folding. In their model, a first phase of deformation produced tight to isoclinal folding of basement and cover rocks and imposed a flattening fabric on them. Porphyritic adamellites (K-granites) intruded as sheet-like bodies and experienced two successive folding episodes of regional extent, producing a complex dome-and-basin configuration, with the less competent overlying greenstone sequences pinched down as synformal structures between the antiformal batholiths. A major difference between the two scenarios is the timing of deformation in relation to intrusion of the batholiths. Regional cross-folding according to Snowden (1984) takes place during and after emplacement of the latest granitoids; deformation following Ramsay (1989) is related to the successive emplacement and expansion ('ballooning') of granitoid suites.

Studies of the strain pattern not only facilitate the determination of the nature of deformation (e.g. Ramsay & Huber 1983), but also allow comparison of finite

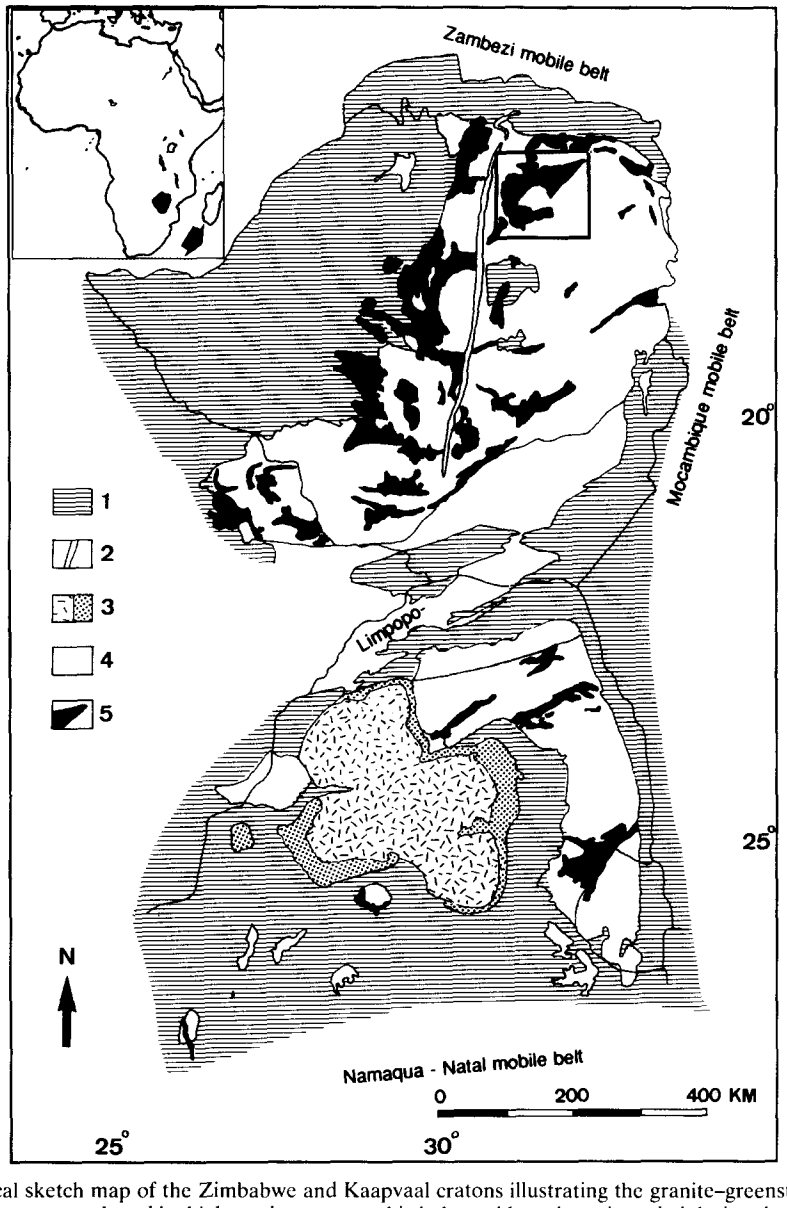

Fig. 1. Geological sketch map of the Zimbabwe and Kaapvaal cratons illustrating the granite–greenstone configuration. The cratonic areas are enveloped by high-grade metamorphic belts and have been intruded during the Proterozoic era by the Great Dyke in Zimbabwe and the Bushveld Complex in South Africa (after Anhaeusser & Viljoen 1986). Legend: 1. Post-Archean cover; 2. Great Dyke; 3. Bushveld Igneous Complex; 4. Archean granite–gneiss terrains; 5. Archean greenstone belts. Box indicates location of Harare–Shamva greenstone belt (Fig. 2).

strains in experimental and natural diapiric structures. The strain pattern developed is an important criterion to distinguish between different processes that may have operated during granite–greenstone belt tectonism (e.g. Dixon 1975, Schwerdtner *et al.* 1978, 1983, Schwerdtner & Troëng 1978, Mareschal & West 1980, Brun & Pons 1981, Ramberg 1981, Soula 1982, Cruden 1988, 1990, Schmeling *et al.* 1988). Quantifying strains in the wall rocks of batholiths can lead to a better understanding of emplacement mechanics (Cruden 1988). Strain patterns in batholithic terrains marked by diapiric emplacement are characterized by sub-horizontal oblation in the upper parts of a diapiric structure, by vertical oblate strains in bi-domal synclines and by vertical prolate strains in multiple-domal synclines or cleavage triple points (CTP, Brun *et al.* 1981).

Structural criteria used to identify diapiric structures (e.g. Schwerdtner *et al.* 1978, 1983, Schwerdtner & Troëng 1978, Brun & Pons 1981, Coward 1981, Bateman 1984, Van Den Eeckhout *et al.* 1986, Brun *et al.* 1990, England 1990) include the development of parallel, continuous and contemporaneously developed foliation patterns within batholiths and cover rocks. Structures should develop conformable to the batholith–cover interface. Strain intensity increases towards the contact; foliations developed during diapirism are most intense near the contact and diminish in intensity at greater distances from it. With increasing maturity of the diapir, shear zones will develop along the contact which indicate a dome-up sense of movement. The stretching lineation pattern developed is radial or tangential to the diapiric body, as opposed to the straight lineation trajectories developed across the midlines of domes produced by interference folding. Porphyroblastesis in the aureole

of diapiric structures is syn- to post-kinematic. Several of these criteria are, however, equivocal and can be associated with diapiric plutons emplaced at various stages of regional deformation (pre-, syn- and post-kinematic; Patterson & Tobisch 1988, Paterson *et al.* 1989).

In the present paper regional structural observations and 30 three-dimensional strain analyses from the Bindura–Shamva greenstone belt, including wall rock strains adjacent to the Chinamora batholith, are presented. The study focuses on the relationship between the deformation of the granitoids and the deformation of the greenstone belt sequences. Opposing tectonic models for the greenstone belt will be tested with the acquired data: (1) cross-folding (Snowden & Bickle 1976, Snowden & Snowden 1979, Snowden 1984); (2) pre-, syn- or post-kinematic plutonism; (3) pluton diapirism and/or ballooning plutonism (Ramsay 1989).

GEOLOGICAL SETTING

The Bindura–Shamva greenstone belt

The Bindura–Shamva greenstone belt, located 80 km north of Harare, forms part of the Harare–Shamva greenstone belt, wrapped around the Chinamora batholith (Fig. 2). The greenstone belt belongs to the western succession of the late Archaean (2.7–2.5 Ga) Upper Greenstones of the Zimbabwe craton, formed on a sialic basement (Wilson *et al.* 1978). The main stratigraphic division of the belt includes the basal Bulawayan Group and the overlying Shamvaian Group (Wilson *et al.* 1978). The Bulawayan Group, which occupies the flanks of the belt, is a thick metavolcanic pile with felsic flows and intrusives, massive and pillowed tholeiitic basalts, komatiitic basalts and serpentinites as well as intercalations of banded iron formations, quartzites, marbles and some clastic metasediments. The younger Shamvaian Group occupies the core of the belt. The contact between the two Groups is an angular unconformity and is frequently tectonically disturbed. A distinction can be made between a felsic metavolcanic dominated lower Shamvaian unit in the southern part of the belt (pyroclastic and volcanic–clastic sediments) and an unconformably overlying metasediment-dominated upper Shamvaian unit in the northern area. The latter unit comprises a basal polymict conglomerate horizon, characterized mainly by granitic boulders and pebbles, poorly-sorted arkoses, (pebbly-) greywackes and pelites. Several complete Bouma sequences have been recognized, indicating a turbiditic depositional environment (Stidolph 1977). Sedimentation was accompanied by the intrusion of high level porphyries.

Metamorphic estimates for the greenstone sequences were obtained using the Grt–Bt, Grt–Crd, Grt–St, Grt–Hbl, Crd–Bt, Am–Pl and Am–Cpx geothermometers (Jelsma work in preparation). Thermometric results show: (A) an increase in peak metamorphic temperatures from 450 ± 25°C (greenschist facies conditions) in central, static-style domains in between three batholiths (triple points), to 550 ± 25°C in the central part of the flanks, to 600–650°C (upper amphibolite facies conditions) in more intensely deformed, dynamic-style domains pinched between two batholiths (the Nyagonde and Umwindsi extensions) and along the interface with the batholiths; (B) a concentric pattern of metamorphic isograds around the batholiths and a gradual increase in metamorphic conditions towards the batholiths. Preliminary barometric results (Grt–Pl–And/Sil and Grt–Pl–Am geobarometers) show a peak metamorphic pressure of 2–3 kbar. Metamorphic mineral assemblages and garnet zoning profiles reveal a clockwise *PT* path of almost isobaric heating, with peak metamorphic conditions being reached during and after the main phase of deformation.

Granitoids

Bordering batholiths for the Bindura–Shamva greenstone belt are Chinamora (to the southwest, radius ≈ 20 km), Mrewa (to the south-east, radius > 40 km) and Madziwa (to the north, radius ≈ 18 km). The composite Chinamora batholith has a sub-elliptical shape (50 × 40 km), with its long axis trending E–W. Field relations indicate a normally zoned intrusion sequence of (1) tonalite ± granodiorite ± granite (gneiss), (2) granodiorite ± granite (gneissic granite) and (3) adamellite (granite) (Snowden & Snowden 1979, Ramsay 1989). Similar compositional intrusion sequences have been observed within the other two batholiths (Stidolph 1973, 1977; cf. Fig. 2). The Madziwa batholith, comparable in size to the Chinamora batholith, shows a reversely zoned intrusion sequence. The Mrewa batholith, larger in size, shows a normally zoned intrusion sequence. Gneisses and gneissic granites (s.l.) of the three batholiths include heterogeneous/banded medium-grained gneisses and migmatites and homogeneous coarse-grained augen gneisses of tonalitic, granodioritic and granitic composition. The gneissic foliation, which increases in intensity outwards, is parallel to the batholith–greenstone interface and fans into the main foliation in the greenstone sequences. This gneissic foliation is subparallel to a weak magmatic foliation, formed by alignment of idiomorphic microcline megacrysts, in the outer parts of the sheet-like adamellites.

Contacts between the various granitoids are intrusive and the younger members contain xenolithic remnants of greenstone belt rocks and previously consolidated igneous rock (Ramsay 1989, fig. 13). The presence of a strong fabric in tonalitic xenoliths within coarse-grained (porphyritic) adamellites implies that the main deformation of the tonalite took place before emplacement of the adamellite. Xenoliths are increasingly flattened and the gneissic foliation increases in intensity towards the batholith margin. The foliation passes into a mylonitic foliation or shows 'lit-par-lit' replacement at the gneiss–greenstone interface. Adamellite–greenstone contacts, on the other hand, are faulted or intrusive. Small mylonite zones have developed in the outer gneissic zones of the Chinamora and Mrewa batholiths.

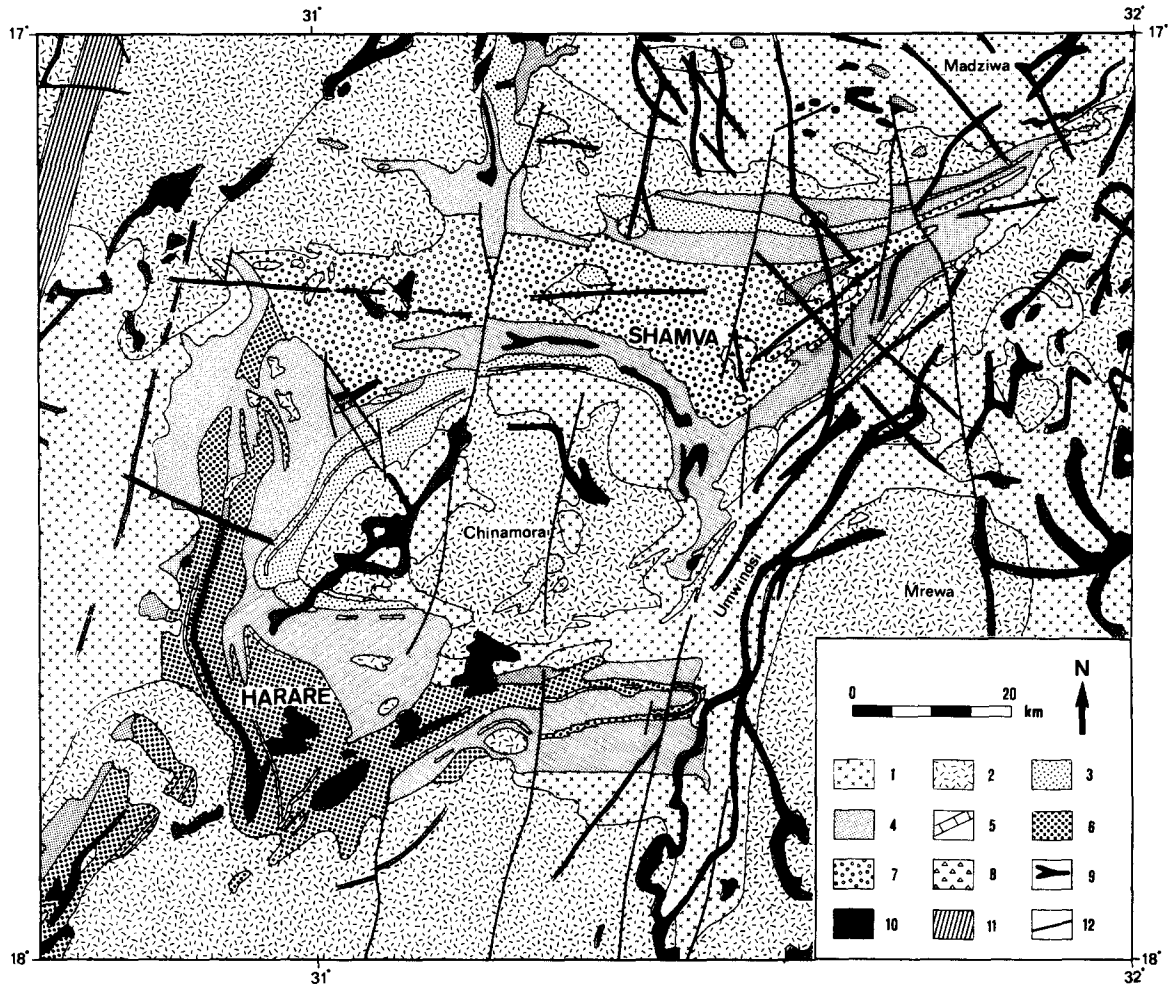

Fig. 2. Geological map of the Harare–Shamva greenstone belt and surrounding granite–gneiss terrains. Legend: *Granite–Gneiss Terrains*. 1. Gneiss and gneissic granite (tonalite–granodiorite–granite); 2. granodiorite and granite (adamellite). *Bulawayan Group*. 3. Felsic metavolcanics (Iron Mask Formation); 4. mafic metavolcanics with intercalated metasediments (Arcturus, Mungari, Nyamwanga and Grahamsdale Formations); 5. Banded Iron Formation; 6. felsic metavolcanics and metasediments (Passaford Formation). *Shamvaian Group*. 7. Felsic metavolcanics (Lower Shamvaian Unit) and clastic metasediments (Upper Shamvaian Unit); 8. mafic metavolcanics. *Other*. 9. Serpentinite, (ultra)mafic complex; 10. dolerite and gabbro; 11. serpentinite and pyroxenite (Great Dyke); 12. fault (modified from Zimbabwe Geological 1:1,000,000 map (7th edn, reprinted) 1985).

Geochronological record

A compilation of geochronological data for the Harare–Shamva area is given in Table 1. Rb–Sr isotope ages disturbed by later thermal and tectonic events are not shown. The age of the Bulawayan Group metavolcanic sequence is (poorly) constrained by Sm–Nd ages (T_{chur}) between 2742 Ma (lower felsic metavolcanics) and 2659 Ma (upper felsic metavolcanics). Within the Umwindsi area, in between the Chinamora and Mrewa batholiths, large gneissic remnants give a Rb–Sr errorchron age of 2865 ± 135 Ma. On the basis of geochronological evidence obtained elsewhere (Wilson 1979) and field evidence (Baldock & Evans 1988) these gneisses have been described as possible basement to the greenstone sequences. Younger ages, a Rb–Sr age of 2688 ± 138 Ma and a U–Pb zircon age of 2667 ± 15 Ma, have been obtained for granodioritic and granitic gneisses of the eastern and northeastern margin of the Chinamora batholith. Adamellite plutons and granodiorite stocks which intrude the greenstone belt (both Bulawayan and Shamvaian Group rocks) have been dated between 2600 and 2500 Ma. Deposition of the Shamvaian Group sediments pre-dates this late magmatic event.

STRUCTURAL ANALYSIS

Greenstones

The main structural elements mapped within the metavolcanics and metasediments comprise: (1) the bedding (S_0), (2) a penetrative schistosity (S_1), a group of folds (F_1) and a strong mineral lination (L_{min}) (Table 2). The bedding (S_0) is recognized by compositional variation on cm and dm scale and locally preserved sedimentary structures (e.g. cross-bedding, channels, convolute bedding, slumps). The S_1 schistosity is defined by alignment of biotite and hornblende and is generally parallel to S_0 (Fig. 3). S_0 and S_1 follow the outlines of the batholiths (Fig. 4a). Younging directions (indicated by pillow basalt geometries, cross-bedding and growth

Table 1. Geochronological data for the Harare–Shamva greenstone belt

Zimbabwe craton		
Great Dyke	2460 ± 16 Ma[1]	
Granite emplacement (Chilimanzi Suite)	<2600 Ma[2]	(Adamellite)
Inter-Montane Basin Formation (Upper Shamvaian Unit)	<2675 Ma	(Turbidites)
Pluton diapirism, ballooning plutonism	2667 ± 15 Ma[3] 2688 ± 138 Ma[4a]	(Granitic gneiss) (Granodioritic gneiss)
Intra-continental rifting (bi-modal Bulawayan Group)	2659 ± 38 Ma[5] 2662 ± 45 Ma[4b] 2717 ± 35 Ma[4c] 2742 ± 38 Ma[4d]	(Arcturus rhyolite) (Passaford dacite) (Passaford dacite) [Iron Mask dacite)
Sialic basement (???)	2865 ± 135 Ma[4e]	(Granodioritic gneiss)

References: [1]Hamilton 1977 (Rb–Sr whole-rock); [2]Vinyu work in preparation (Rb-Sr whole rock); [3]Jelsma *et al.* work in preparation (U–Pb zircon); 4. Baldock & Evans 1988 ([a-e] Rb–Sr whole-rock; [b–d]Sm–Nd whole-rock); [5]Taylor *et al.* 1991 (Pb–Pb whole-rock).

laminations in stromatolites) within the flanks of the belt point towards the core, implying that the structure is a large-scale synclinorium with an overturned northern limb. The opposing younging directions occasionally found within the flanks are due to small-scale secondary folds. In the Bindura, Shamva and Nyanji areas macroscopic gently plunging F_1 folds were recognized. Axial planar traces of these folds define a polygonal structure. The style and wavelength (λ) of the F_1 fold structures varies across the greenstone belt, reflecting variations in strain intensity. The outer zone of the Shamvaian Group shows mesoscopic tight-isoclinal non-cylindrical folds with $\lambda \leq 100$ m. S_0, S_1 and axial planar traces of F_1 are (sub)parallel to each other. The central axial zone of the synclinorium shows macroscopic, open-tight near-cylindrical fold structures, e.g. the Panmure antiform ($\lambda \approx 1$–2 km). S_0 and axial planar traces of F_1 are (sub)parallel to each other, but folding took place without the development of S_1.

The poles to S_0 and S_1 for the Shamvaian Group define almost common great circles, perpendicular to the trend and plunge of B_1 hingelines of mesoscopic folds (Figs. 4b & c). The hingelines of the folds (Fig. 5c) plunge parallel to mineral lineations (defined by amphibole) at moderate angles westward in the Shamva area, eastward in the Bindura area and at steep angles northward in the Nyanji area. Hence, the S_0 and S_1 planar elements define a macroscopic pattern which can be described as an inward steepening triangular synform or cleavage triple point (CTP). Linear elements (i.e. B_1 hingelines and mineral lineations, L_{min}) plunge towards the centre of this structure (Figs. 3 and 4). The absence of any deformational imprint or cross-cutting relationship indicates a contemporaneous development of all F_1 folds. The configuration shown in the central part of Fig. 4(a) resembles the curtain folds described by Talbot & Jackson (1987) and can only be explained by vertical biaxial constrictional strain.

Table 2. Structural elements encountered in the study area

Planar elements:	
S_0	Bedding, with locally preserved sedimentary structures (e.g. channels, slumps, pillows)
S_1	penetrative schistosity, defined by alignment of biotite and amphibole; axial planar trace of F_1 folds
S_2	weak schistosity, defined by alignment of biotite and amphibole; axial planar trace of F_2 folds
S_s	shear foliation
Linear elements:	
B_1	hingeline of F_1 folds
L_{min}	mineral lineation (amphibole)
L_x	longest axis of strain ellipsoids
L_s	stretching lineation within shearzones
B_s	hingeline of shear-folds, developed within marginal zones of the greenstone belt

Both the northeastern and southern extensions of the greenstone belt (Nyagonde and Umwindsi areas, Fig. 3) suffered local refolding of F_1 folds about F_2 axes. A weak S_2 schistosity, defined by alignment of biotite, occurs in some of the greenstones and adjoining gneisses. These structures are interpreted as wrench folds initiated by differential lateral movements between adjacent batholiths, as exemplified by left-lateral shear along the Umwindsi shear zone (USZ). The USZ is a high strain domain of variable width, striking, NNE–SSW along the eastern side of the Umwindsi greenstone belt extension (Fig. 3). A 100–200 m wide mylonite zone shows gently southwestward-plunging stretching lineations and an oblique left-lateral sense of movement (Huizenga unpublished internal report 1991). The shear zone is less than 10 km long and probably did not accommodate large displacements. It grades into the highly strained outer parts of the Chinamora and Mrewa batholiths. Along the margins of the Umwindsi greenstone belt extension migmatites are exposed that might have formed during emplacement by partial melting of the wall rocks.

Within the greenstone belt, steep, ENE-striking shear zones (cataclasites and mylonites) trend parallel to the traces of S_0 and S_1 and cut across F_1 folds (e.g. in the Shamva mine, Fig. 3). The shear zones converge towards the highly strained northeastern part of the belt. Stretching lineations are (sub-)horizontal or plunge westward at moderate angles. The sense of shear is

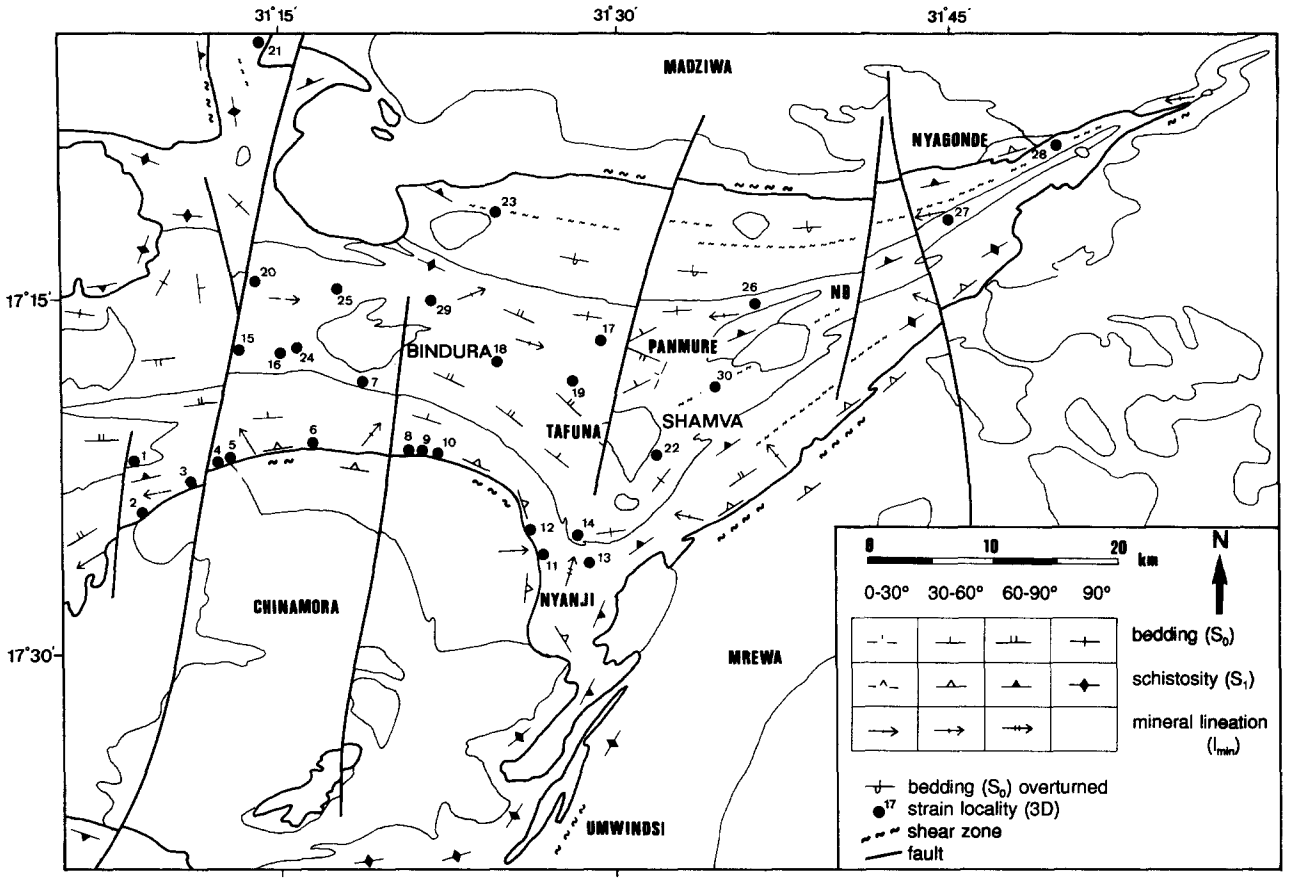

Fig. 3. Structural map of the Bindura–Shamva greenstone belt. The localities of strain analysis (1–30) are indicated. See text for discussion.

generally left-lateral, with variable reverse oblique components. Gold mineralization is associated with several of the major shear zones (e.g. Shamva–Cymric and New Brixton mines; Jelsma *et al.* 1990).

Chinamora and Mrewa batholiths

Along the contact of the greenstone belt with the northern margins of the Chinamora and Mrewa batholiths a shear foliation is developed in the country rocks and granitoids, varying strongly in intensity with lithology. This shear foliation is developed in a zone up to 500 m across; (sub)parallel to the S_0 and S_1 foliation and parallel to the granite–greenstone interface. It is characterized by a shallow (20–45°) northerly-dipping penetrative schistosity, anastomosing around clasts and phenocrysts (quartz, feldspar) on a meso- to microscopic scale. In cross-sections, lithological boundaries and the foliation show a fan shape, the dips being shallow near the marginal zones and becoming increasingly steeper towards the greenstones. Porphyroclasts of andalusite and staurolite are often encountered in volcanic schists and have grown pre- to syn-kinematically with respect to a phyllonitic foliation. The schistosity shows deflection around slightly elongated porphyroclasts. Recumbent folds with an off-the-dome vergence, porphyroclasts with asymmetric recrystallized tails and *S–C* mylonites in the granitoids indicate a (oblique) normal, dome-side-up sense of movement. In marbles and banded ironstones, shear folds commonly show sub-horizontal or gently plunging fold axes. Mineral lineations and quartz rods at the northern and northeastern contact of the Chinamora batholith are oriented radially outwards but diverge towards an orientation obliquely tangential to the interface towards the west (Figs. 3 and 5a). Extension directions of boudinaged quartz veins are oriented tangentially to the bedding. Along the straight contact with the Mrewa batholith, linear elements, i.e. fold axes of sheath and oblique folds (Ramsay 1980), mineral lineations as well as extension directions of boudinaged quartz veins, plunge at a low angle (30–50°) towards 280–300° (Fig. 5b).

Madziwa batholith

Two generations of shear zones occur along the contact with the Madziwa batholith (Fig. 3). A vertical shear foliation is developed in the marginal zone of otherwise unfoliated granites. The shear zone is approximately 20 m across and continuous over 50 km. Stretching lineations are subhorizontal. An early generation of shear zones along this interface is restricted to the Nyagonde area, the northeastern part of the greenstone belt. Shear planes of these high-angle reverse faults dip at 40° towards the batholith. Stretching lineations plunge at 40° towards 340° and shear indicators show a dome-up sense of movement, possibly related to the overturning of the northern flank. Basal successions of the Maparu

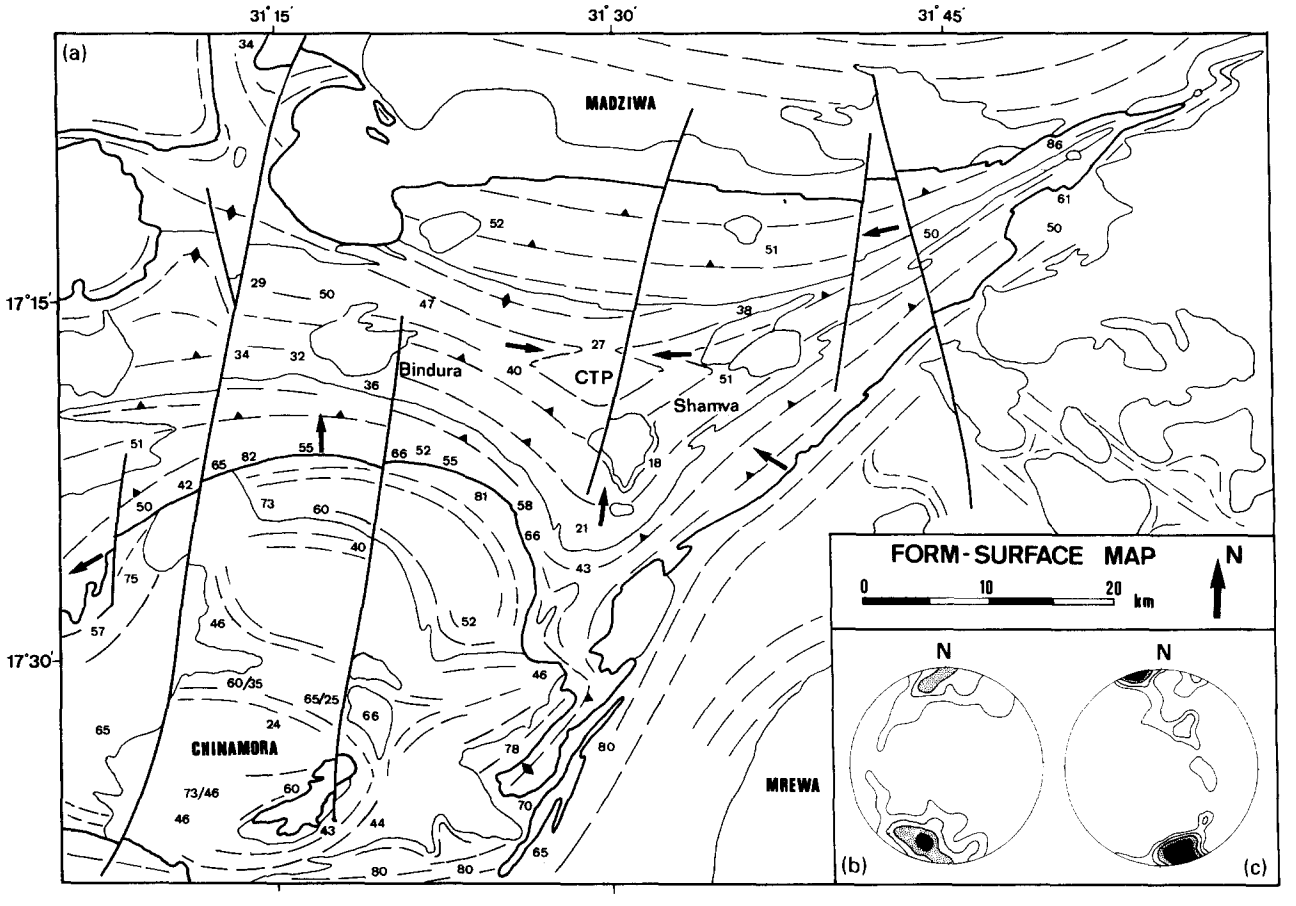

Fig. 4. (a) Form-surface map of the Bindura–Shamva greenstone belt, showing foliation trajectories (triangles indicate dip direction of foliation) and lineation trends (bold arrows). CTP: cleavage triple point; numbers indicate percentage shortening across the Z-axis of strain ellipsoids. (b) Lower-hemisphere equal-area projections for poles to the S_0 and S_1 foliations (density distributions) within Shamvaian sediments for the Bindura area (n = 93; 1,3,5,7× uniform distribution) and (c) the Shamva area (n = 221; 1,3,5,7× uniform distribution).

formation felsic metavolcanics (Fig. 2) show several zones of ductile deformation where rocks are mylonitized and shear bands and shear folds are developed. Pillow basalts within the uppermost sequences of the underlying Mungari formation are strongly flattened. Longest axes of the triaxially flattened strain ellipsoids plunge steeply towards a similar direction (340°), oblique to mineral lineations in the eastern part of the greenstone belt.

STRAIN ANALYSIS

Three-dimensional strain analyses have been performed on outcrops at 30 localities within the core and the flanks of the greenstone belt. Analyses have been performed on a variety of rock types, comprising conglomerates (mainly granitoid clasts; some basaltic clasts), pillow basalts and agglomerates. In addition, at 11 localities within the batholiths, two-dimensional strain analyses have been performed on xenoliths, on (sub)horizontal planes. A comparison will be made with 80 two-dimensional strain ellipsoids (xenoliths) for the Chinamora batholith, described by Ramsay (1989).

Procedure

Strain measurements were performed in the field by measuring the axial ratios and the pitch of the longest axis of a number of elliptical strain markers within a plane of known orientation. Where more than 15 measurements could be made on one plane, a strain ellipse R_s was calculated by means of the R_f/ϕ method (Ramsay 1967, Dunnet 1969) using the algebraic formulae of Shimamoto & Ikeda (1976). Where less than 15 measurements were made on one plane, R_s was estimated by calculating the harmonic mean of the ratios of the ellipses (c.f. Lisle 1977). The two-stage procedure from Owens (1984) was used to determine the best-fit ellipsoid from elliptical sections on three or more oblique planes (Van Balen & Van Wees unpublished internal report 1987). The type and intensity of the strain are characterized by the k- and d-values of the strain ellipsoid, respectively (Flinn 1962, Ramsay & Huber 1983, pp. 199–205);

$$k = \frac{(R_{xy} - 1)}{(R_{yz} - 1)} \quad (1)$$

$$d = \sqrt{(R_{xy} - 1)^2 + (R_{yz} - 1)^2}. \quad (2)$$

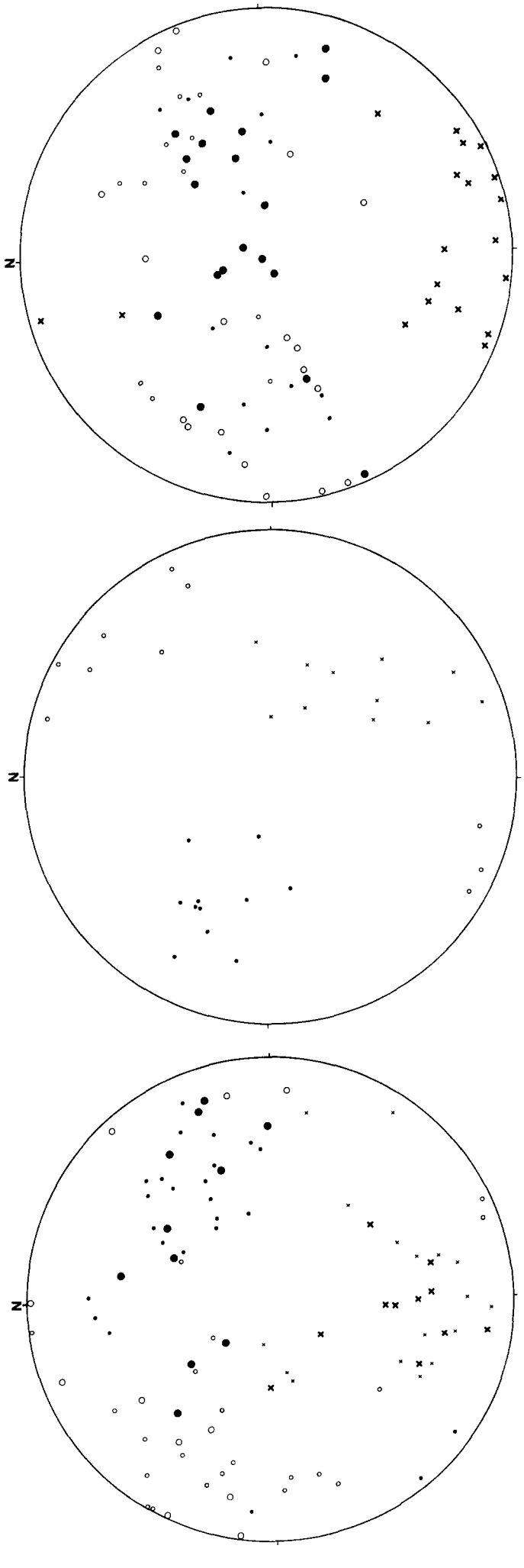

Fig. 5. Lower-hemisphere equal-area projections for linear elements, and X, Y and Z principal axes of strain ellipsoids for (a) the Chinamora wall rocks, (b) the Mrewa wall rocks and (c) the interior of the greenstone belt. Key: ●, X-axis of strain ellipsoid; ○, Y-axis of strain ellipsoid; X, Z-axis of strain ellipsoid; •, mineral lineation L_{min}; × pole to foliation; ○, Y-axis constructed from L_{min} and pole to foliation.

Table 3. Results of strain analyses

Location	L	*n*	*XY*	*X*	*X/Y*	*Y/Z*	*k*	*d*	*x*	BAWE	*X* (%)	*Y* (%)	*Z* (%)
1. Wolf hill	(c)	32	009/77	319/70	1.53	2.33	0.40	1.43	4.0	0.41	76	15	−51
2. Kasipa	(a)	26	325/41	310/40	1.71	2.17	0.61	1.37	1.5	0.28	86	9	−50
3. Mawu river	(a)	42	349/54	056/29	1.49	1.85	0.58	0.98	0.2	0.19	60	8	−42
4. Gosforth	(c)	35	358/61	322/56	1.67	3.76	0.24	2.84	0.2	0.30	117	30	−65
5. Wiseacre	(c)	45	358/54	035/48	7.02	5.10	1.47	7.28	0.2	0.33	527	−11	−82
6. Brinkburn	(a)	39	004/42	070/20	1.73	2.53	0.48	1.70	0.3	0.17	97	14	−55
7. Coach H.	(c)	60	022/85	295/34	1.47	1.63	0.74	0.79	5.1	0.03	53	4	−36
8. Hildadale	(c)	60	013/60	070/43	2.81	3.03	0.89	2.97	0.7	0.04	187	2	−66
9. Kingston	(c)	30	004/39	010/39	1.56	2.45	0.39	1.55	0.6	0.37	81	16	−52
10. Atherstone	(c)	50	025/55	025/55	1.73	2.51	0.47	1.68	0.3	—	97	14	−55
11. Glamorgan	(p)	23	092/30	090/30	1.80	3.70	0.30	2.82	0.2	0.27	128	27	−66
12. The Vale	(c)	51	038/20	072/17	1.69	2.75	0.39	1.88	0.2	0.37	99	18	−58
13. Woodlands	(c)	63	017/70	075/56	1.36	2.01	0.36	1.74	4.0	0.11	55	14	−43
14. Hereford	(c)	67	007/89	092/73	1.68	1.09	9.71	0.69	3.5	0.07	45	−14	−21
15. Simoona	(c)	80	358/83	020/82	2.01	1.30	3.37	1.05	9.0	0.03	73	−14	−34
16. Insingisi	(c)	60	028/53	108/13	1.30	1.56	0.54	0.64	8.0	0.06	38	6	−32
17. Nzua	(c)	50	348/89	343/89	1.42	1.36	1.17	0.55	13.0	0.01	39	−2	−27
18. Barassie	(c)	59	017/57	333/49	2.50	1.30	5.00	1.53	7.5	0.13	102	−19	−38
19. Usaramo	(c)	65	011/60	062/47	1.51	1.84	0.61	0.98	9.0	0.10	62	8	−42
20. Jesmond D.	(c)	47	164/83	081/47	1.35	1.42	0.84	0.55	12.0	0.15	38	2	−29
21. Argle Park	(p)	16	054/63	143/03	1.13	1.74	0.18	0.75	0.3	0.15	31	16	−34
22. Walwyn	(c)	120	308/62	253/47	1.60	1.06	9.96	0.60	7.0	0.01	39	−13	−18
23. Mt. View	(c)	18	023/86	111/25	2.14	2.10	1.03	1.58	4.0	0.05	112	−1	−52
24. Redlands	(c)	20	160/53	247/03	2.47	2.35	1.09	2.00	12.0	0.11	142	−2	−58
25. Mazoe W.	(c)	30	332/81	055/39	3.28	1.53	4.28	2.34	12.0	0.05	154	−22	−50
26. Mazoe Isl.	(c)	30	343/88	071/37	1.09	1.96	0.10	0.96	9.0	—	33	22	−38
27. Chiwore	(c)	82	340/73	340/73	1.00	2.82	0.00	1.82	4.0	—	43	43	−50
28. Nyagonde	(p)	64	342/76	340/75	3.92	10.25	0.32	9.70	0.8	0.05	437	37	−86
29. Melfort	(a)	15	360/78	052/48	3.60	1.37	7.00	2.60	11.0	—	161	−28	−47
30. Shamva	(a)	20	335/90	246/83	1.37	2.43	0.26	1.48	9.0	—	65	20	−51
31. Mumurgwi	(x)	25		092		2.50							
32. Umwindsi	(x)	20		025		4.30							
33. Rutope	(x)	20		035		5.62							
34. Rutope	(x)	31		045		5.25							
35. Double-S	(x)	10		066		7.00							
36. Frascati	(x)	7		060		5.21							
37. Frascati	(x)	20		050		4.53							
38. Katiyo	(x)	10		040		—							
39. Katiyo	(x)	15		055		3.13							
40. Katiyo	(x)	15		043		2.50							
41. Katiyo	(x)	12		158		4.16							

Parameters shown are localities, lithologies (L) (c = pebbles, conglomerate; a = volcanic bombs, agglomerate; p = pillow basalt; x = xenoliths, granitoids); number of measurements (n); dip of the XY-plane (XY); plunge of the longest axis (X); X/Y and Y/Z ratios of the strain ellipsoid; k- and d-values of the strain ellipsoid; distance to the nearest batholith (x); BAWE factor; and total strain across X-, Y- and Z-axes (%).

The fit of the calculated strain ellipsoid to the data input is expressed by the BAWE factor (Van Balen & Van Wees unpublished internal report 1987), which corresponds to the mean misfit between predicted and observed elliptical sections, i.e. the proportion of the area of two ellipses that does not overlap when they are projected on a common midpoint:

$$\text{BAWE} = \sum_{j=1}^{n} \frac{M_{cj} + M_{oj}}{A_{cj} + A_{oj}} \Big/ n, \qquad (3)$$

where A_0= area of the observed ellipse, A_c= area of the calculated ellipse, M_0 = area of observed ellipse that does not overlap the calculated ellipse and M_c= area of calculated ellipse that does not overlap the observed ellipse. The BAWE factor can have a pronounced effect on the k-value and the orientation of the ellipsoid. Measurements with BAWE factor > 0.4 should be regarded as unreliable, especially for low d-values. Since the BAWE factor is calculated for normalized ellipses, the effect on the d-value is much less pronounced.

The R_f/ϕ method assumes that the strain markers were of truly ellipsoidal shape with random orientation in the undeformed state and behaved passively during deformation. Although most of the strain markers are rheologically similar to their surroundings (pebbles, pillow basalts, volcanic bombs), some of the analysed strain markers might have been less subject to volume change and total flattening than the matrix in which they are embedded (conglomerate, basalt, agglomerate), and did not behave entirely passively. This would lead to an underestimate of the amount of strain.

Results

The results of the strain analyses are summarized in Table 3 and depicted graphically in a Flinn diagram in Fig. 6(a). The ratios $a = X/Y$ and $b = Y/Z$ have been calculated assuming isochoric strain. In order to assess volumetric effects (Ramsay & Wood 1973) a logarithmic Flinn diagram is included (Fig. 6b). Strain data from the wall rocks of the Chinamora and Mrewa batholiths are shown in stereograms in Figs. 5(a) & (b) and from the interior of the greenstone belt in Fig. 5(c). The stereo-

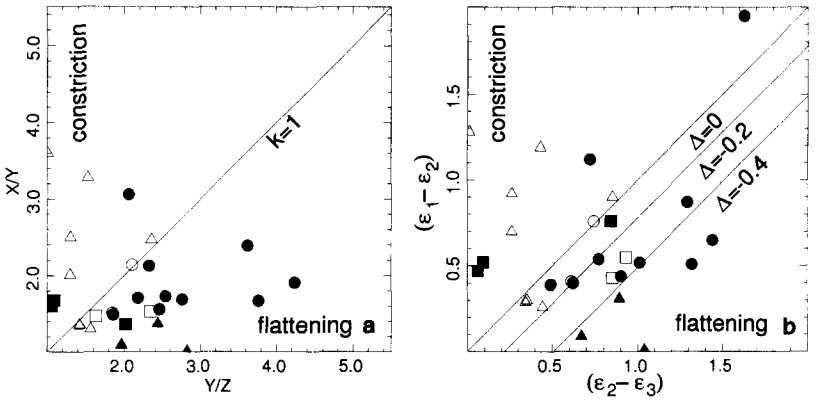

Fig. 6. Results of the strain analyses for different areas plotted in (a) a Flinn diagram and (b) a logarithmic Flinn diagram. Symbols denote samples from different subareas: ● Chinamora margin; ■ Nyanji area (CTP); ▲ Shamva area; ○ Madziwa margin; □ Bindura area; △ Bindura stock.

grams show that mineral lineations are parallel to the X-axes of the strain ellipsoids, thus representing stretching lineations. Within the greenstone belt, three specific strain zones were distinguished.

(1) Strain ellipsoids within the wall rocks (< 200 m) of the Chinamora batholith show triaxial flattening ($0.3 < k < 0.6$). The d-values of the strain ellipsoids ('surfboard type') are high ($d > 1/5$). The shape of some of the strain markers is asymmetrical, indicating a component of simple shear. Since progressive simple shear (with a vorticity $W_k = 1$; Means *et al.* 1980) leads to plane strain ellipsoids ($k \approx 1$), with X parallel to the shear direction and the XY-plane parallel to the shear plane (Ramsay 1980), the observed triaxially flattened ellipsoids can not be the result of a deformation history of progressive simple shear alone. Triaxial flattening strains can be explained by a deformation path of combined simple shear and pure shear with flattening normal to the shear plane ($0 < W_k < 1$), which is supported by the presence of extensional structures oriented tangentially to the foliation plane.

(2) In the eastern part of the Shamva area, strain ellipsoids are of uniaxial vertical oblate type ($k \approx 0$, 'pancake type'). Further west, towards the open end of the interdomal syncline, plane strain types prevail ($k \approx 1$) and X-axes plunge at moderate angles towards the CTP (Fig. 5c). The d-values of the strain ellipsoids are intermediate, ranging between 1 and 2. In the Bindura area, the strain ellipsoids range from triaxially oblate to moderately prolate types ($k \approx 0.5$–5). X-axes plunge parallel to mineral lineations towards 060–090° at variable angles. Prolate strain ellipsoids were measured on localities near the late intrusive Bindura granodioritic stock.

(3) Highly prolate shapes of ellipsoids ($k \approx 7$–10) have been found in or adjacent to the CTP. Strain intensities in this area, located in between the three batholiths are the lowest encountered in the greenstone belt ($d \approx 0.5$–0.7).

The variation of strain intensity (d-value) and strain type (k-value) for the different strain zones is demonstrated in Fig. 7. The strain intensity increases (i) from the CTP towards the batholith–greenstone interface (Fig. 7a) and (ii) from the CTP to the two wedge-shaped extensions of the greenstone belt (Nyagonde and Umwindsi areas; Fig. 7c). The strain-type varies from triaxial flattening near batholith margins towards uniaxial flattening within saddle culminations (SC) and towards uniaxial constriction within the CTP (Figs. 7b & d).

Strain data for the interior of the Chinamora batholith were adopted from Ramsay (1989), who performed strain analyses within the Chinamora batholith, assuming that the strain is characterized by uniaxial horizontal flattening ($k \approx 0$). Although our measurements for the wall rocks of the Chinamora batholith indicate that strains are characterized by triaxial flattening, our measured total shortening across the Z-axis for the wall rocks of the Chinamora batholith is comparable with the data obtained by Ramsay for the outer zone of the Chinamora batholith (Fig. 8). The measured strains associated with the tightening of the belt indicate that average values of total shortening across the Z-axis increases from less than 30% within the centre of the area to over 80% within marginal zones. Strain analyses (two-dimensional) on xenoliths within tonalitic and granodioritic gneisses, adjacent to the Umwindsi greenstone belt extension, show such strong flattening. High flattening strains are characteristic for the interdomal synclines. The northeastern end of the greenstone belt, for example, shows large boudins of greenstone rocks within the gneisses.

DISCUSSION

The presented structural observations and strain data can be used to discuss the conflicting models for the deformation in the area. The Bindura–Shamva greenstone belt forms a large-scale synclinorium with an S_0 and S_1 foliation generally concordant to the batholith–greenstone interfaces. Within the batholiths, deformation structures such as augen gneiss textures and mylonitic foliations prevail within the gneissic, outer portions and are continuous with the S_1 foliation in the wall rocks. The presence of a penetrative S_1 foliation

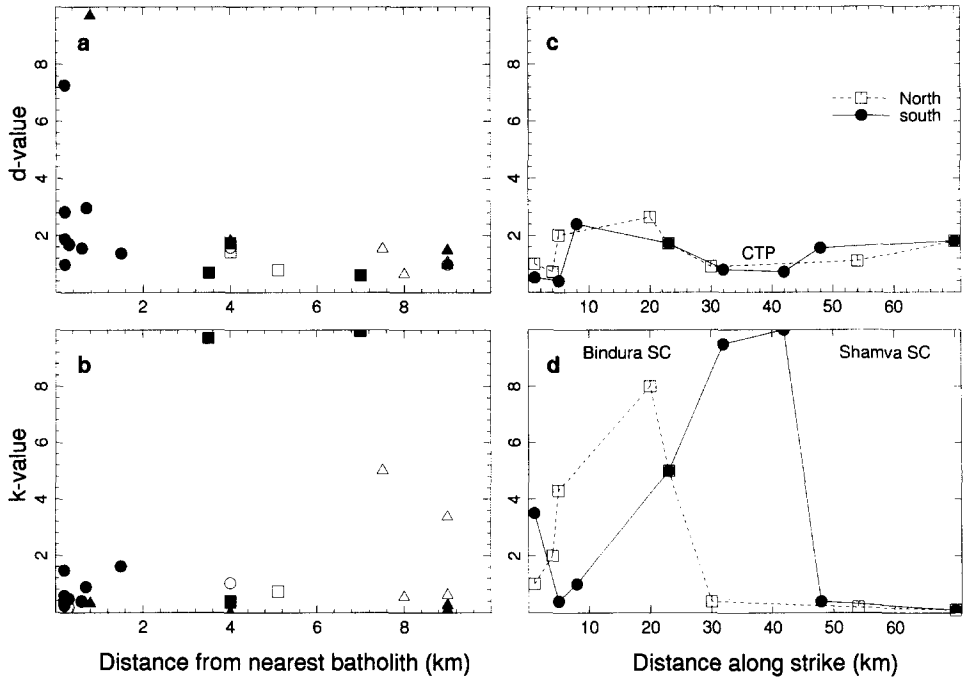

Fig. 7. (a) Strain intensity (d-value) and (b) strain-type (k-value) vs the distance to the nearest batholith–greenstone interface, symbols as in Fig. 6; (c) strain intensity (d-value) and (d) type of strain (k-value) for strain ellipsoids along a northern and a southern E–W profile within Shamvaian sediments.

within marginal zones and of mylonite zones at the actual batholith–greenstone contact is clearly a result of progressive deformation with maximum strain focused at the outer margin of the batholiths. Bulk flattening strains can be expected in greenstone wall rocks and outer portions of batholiths if diapirism is the emplacement mechanism or if final pluton emplacement takes place by ballooning (Ramsay 1989). Yet regional tectonic deformation with rigid pre-tectonic batholiths acting to channel strain–tectonic flow within the greenstones, might also produce high strain gradients near marginal zones and an increase in strain towards pluton margins can also occur around syn-tectonic or forcefully emplaced post-tectonic plutons (Soula 1982, Bateman 1984, Paterson & Tobisch 1988, Brun *et al.* 1990).

Similar to the variations in the strain intensity, the variations in metamorphic conditions also correlate with distance to surrounding batholiths. Contact metamorphic isograds are concentric around the batholiths and pass continuously into regional metamorphic isograds. Metamorphic temperatures show a gradual increase from 450°C near the CTP to 600–650°C along batholith–greenstone interfaces. The growth of syn- to post-kinematic garnet porphyroblasts in lithologies within the outer flanks of the greenstone belt shows that peak metamorphic conditions were reached during and after the main phase of deformation. It also shows a close relationship, with peak of contact metamorphism being contemporaneous with the peak of regional metamorphism and regional deformation.

Snowden & Bickle (1976) explained the strain distribution within the Chinamora batholith with regional deformation *after* emplacement of the youngest granites (adamellites). Contrary to our results, contact metamorphism would be expected to be pre-kinematic and contact metamorphic isograds would be expected to have

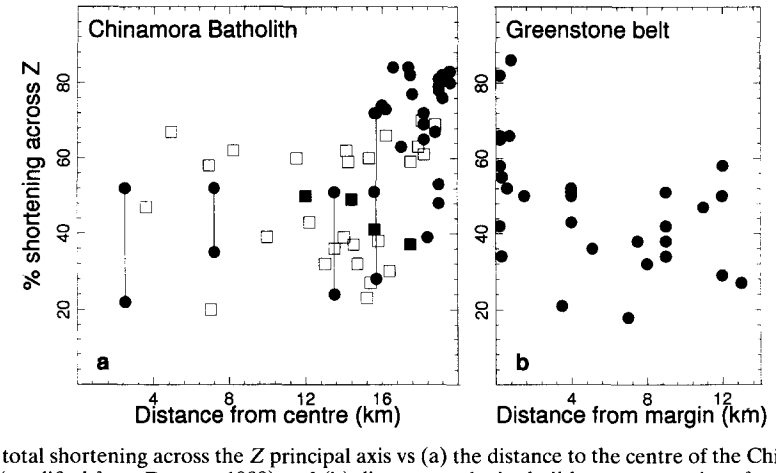

Fig. 8. Percentage total shortening across the Z principal axis vs (a) the distance to the centre of the Chinamora batholith for interior strains (modified from Ramsay 1989) and (b) distance to the batholith–greenstone interface for the envelope strains.

suffered two successive regional folding events. Furthermore, the deflection of microcline megacryst fabrics in porphyritic adamellites around the Inyauri macro-xenolith (roof pendent ?) was used as evidence for (successive) cross-folding *within* the Chinamora batholith (Snowden & Bickle 1976, Snowden & Snowden 1979, Snowden 1984). Deflection of foliations around macro-xenoliths, however, is a common criterion to demonstrate magmatic flow (Paterson *et al.* 1989).

The presence of a triangular foliation pit or CTP, characterized by vertical constrictional strains and low *d*-values, at the open end of three interdomal synclinoria, is consistent with modelling results of Dixon & Summers (1983) and argues against successive fold phases. Interdomal synclinoria (Shamva, Bindura and Nyanji–Umwindsi areas) are characterized by vertical flattening strains ($k \approx 0$). Wall rocks along the northwestern margin of the Chinamora batholith show an oblique tangential stretching lineation pattern, diverging along the northern and eastern margin to a radial pattern. Interference of successive regional fold phases implies a rotation of the regional crustal shortening direction. Strain patterns developed will produce lineation trajectories that converge towards a straight trend across the midlines of domes (Schwerdtner *et al.* 1983, Veenhof & Stel 1991). The diverging subhorizontal lineation trajectories are therefore not compatible with such a tectonic setting. The strain pattern observed conforms to the natural and theoretical strain environments of batholithic terrains marked by diapiric emplacement (Brun *et al.* 1981, Veenhof & Stel 1991). No cross-folds with orientations and characteristics capable of giving rise to the batholith structures have been observed. The concept of a CTP formed as a result of either interference between a local ballooning strain field and a regional strain field (Brun & Pons 1981, Bateman 1984) or forceful emplacement of syn-tectonic plutons (Paterson & Tobisch 1988) is rejected given the structural arguments described above (stretching lineation trajectories and strain pattern). Furthermore, in the former case regional deformation will overprint an older ballooning foliation and in the latter case a CTP will develop only near one of the two ends of the pluton.

Hence, deformation structures (CTPs, SCs, minor structures along highly strained marginal zones and folds produced by magmatic flow around macro-xenoliths), previously ascribed to two successive superimposed deformation phases by Snowden and coworkers, can be explained by single-phase interdomal progressive deformation.

Data for the interior strain distribution of the batholiths are at present known for the Chinamora batholith only, but age constraints, compositional zoning and structural data suggest that a similar emplacement process has operated for the three batholiths. Ramsay (1989) demonstrated ballooning by pointing at discontinuous internal zoning related to strain gradients within different lithologies of the Chinamora batholith and assumed uniaxial oblate strains in marginal zones. The Chinamora wall rocks in this study are shown to be characterized by triaxial flattening strains. Although few strain data were available for the centre of the Chinamora batholith, the complex and irregular fold styles within central xenoliths such as the Inyauri macro-xenolith were interpreted by Ramsay (1989) as resulting from a single phase of constrictional deformation. The theoretical interior strain distribution of granitic diapirs shows a very similar pattern of strong oblate strain at the margins and vertical prolate strains at the centre (Cruden 1988, 1990, Schmeling *et al.* 1988).

The finite strains recorded for the Chinamora wall rocks are of generally lower magnitudes than those predicted by the results of, for example, Cruden (1988) and Schmeling *et al.* (1988). The discrepency between natural and experimental strain data was recorded in observations by Schwerdtner *et al.* (1978) and Tobisch *et al.* (1986) and might be due to (1) the effect of a short strain memory of the greenstone rocks (Means 1981, Talbot 1987) or (2) the concentration of strain in narrow ductile shear zones close to the diapir as a result of differences in rheology as well as thermal and strain softening (Cruden 1988, Schmeling *et al.* 1988). Such shear zones occur along most of the gneiss–greenstone interfaces of the batholiths. Kinematic indicators show dome-upward movements. Folds in the contact zone can be interpreted as cascade folds (off-the-dome vergence), oblique folds and sheath folds. Cascade folds are restricted to the border between rising and subsiding regimes (Dixon & Summers 1983). A consistent dome-side-upward movement around the margin of a batholith is a strong indication for diapiric deformation (Bateman 1984, Van Den Eeckhout *et al.* 1986). The orientation of the shear foliation parallel to the bedding, and the variation in strain intensity in the sheared contact zone imply that the cover has slid off the growing batholiths by a flexural-slip mechanism.

Structural criteria to distinguish pluton diapirism (s.s.) from ballooning plutonism are not common (England 1990). The presence of rotated andalusite and staurolite porphyroclasts in schistose felsic metavolcanics at the batholith–greenstone contact, indicates a syn-kinematic growth. Because the greenstone envelope must be heated before diapiric ascent (Hot Stokes model, England 1990), porphyroblast, growth in the envelope would be expected to be pre- to syn-kinematic. Ballooning deformation would have accompanied thermal metamorphism rather than post-dated it and porphyroblast growth can be expected to be syn- or post-kinematic (England 1990). During final emplacement many diapiric plutons will expand or balloon. The strain data and structural observations, therefore, do not lead to an unambiguous interpretation of the emplacement mechanism of the batholiths. (a) Triaxial flattening strains such as those observed at the granite–greenstone interfaces are not indicative of 'ballooning' as shown by experimental work of Cruden (1988). Triaxial flattening strains can be produced by a combination of simple shear and pure shear (progressive flattening normal to the shear plane), i.e. the diapir has to push material outwards and drag it upwards to get through. (b) Radial

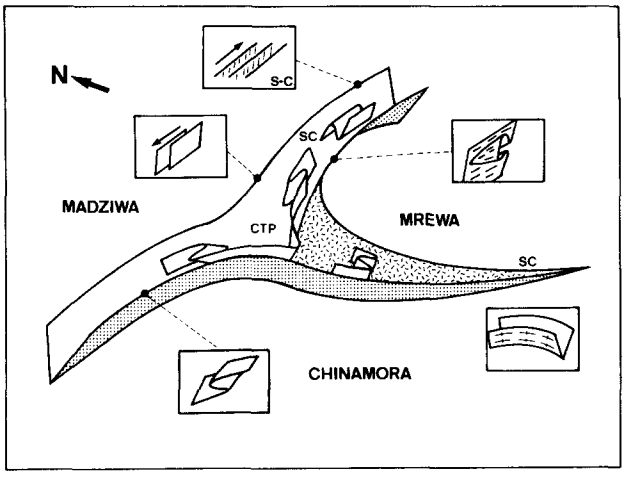

Fig. 9. Schematic block diagram for the Bindura–Shamva greenstone belt, showing the developed cleavage triple point (with curtain folds), saddle culminations, fold styles and surrounding batholiths. Not to scale.

patterns of linear elements in the wall rocks are best explained by diapirism whereas tangential lineations and tangential extensional structures (horizontal stretching) may be related to (local ?) pluton expansion in the sense of Brun & Pons' (1981) 'mongolfier' model. (c) The cover sliding off-the-dome kinematics can be used as an argument for diapirism, although a ballooning pluton also has to push upwards as well as outwards (expanding), implying local dome-side-up kinematics on upper flanks. 'Lit-par-lit' replacement at gneiss–greenstone contacts is a strong argument for ballooning plutonism (progressive bulk shortening). (d) Discontinuous internal strain gradients and discontinuities in the intensity of the development of foliations and solid-state micro-structures across internal contacts of generations of plutons are also best explained by ballooning of a pluton.

We therefore suggest that vertical tectonism was the main tectonic driving force, with deformation being related to a combination of pluton diapirism and ballooning plutonism. A single-phase interdomal progressive deformation solves the problem of the lack of an F_2 (or F_3) imprint on the greenstone sequences. Structures such as CTPs and CSs are formed during emplacement and subsequent expansion of the batholiths (Fig. 9).

The presence of a strong fabric in tonalitic xenoliths in adamellitic granites implies that the main diapiric deformation took place before emplacement of the adamellites. The truncation of regional structures by adamellite pluton margins, the lack of foliations or strain in these plutons, the post-kinematic growth of porphyroblasts in narrow contact aureoles and particularly the new radiometric ages (Table 1) are criteria which demonstrate that emplacement of these plutons was a late-stage event in the deformation history.

TECTONIC MODEL

The data presented show that pluton emplacement triggered the deformation of the greenstone sequences and that the deformation history was single-phase progressive rather than polyphase. The characteristic structural and strain patterns within cleavage triple points (CTP), interdomal synclinoria (SC) and wall rocks demonstrate interference of strain fields developed around batholiths (diapiric structures). The results support a tectonic model in which deformation is related to remobilization of a buoyant substrate of sialic composition and diapiric emplacement of granitoid plutons. This substrate may have been an extensive sheet of granitoid batholiths which intruded at depth below a greenstone cover and which was subsequently remobilized into diapiric domes. Such a sheet of batholiths was predicted by Dixon & Summers (1983) and Ridley & Kramers (1990) and might be envisaged to have triggered the diapiric emplacement of a number of batholiths in Zimbabwe. The strain data and structural observations do not lead to an unambiguous interpretation of the emplacement mechanism. Some of the features are best explained by pluton diapirism, others by ballooning plutonism. Emplacement of adamellite plutons postdated the major deformational events. Future high-precision U–Pb zircon geochronology (Jelsma *et al.* work in preparation, Vinyu work in preparation) will better contrain the time span of these processes.

Acknowledgements—We thank Laszlo Westra and Jan Kramers, project leaders of MINREST, for the organization and valuable discussions, and Jacques Touret, Tom Blenkinsop, Harry Stel and Henk Helmers for providing constructive criticism. R. W. England and an anonymous reviewer are greatfully acknowledged for numerous useful comments. This research forms part of the MINeral RESearch and Training (MINREST) Program, a co-operation project between the Institute of Earth Sciences, Free University, Amsterdam, The Netherlands, and the Department of Geology, University of Zimbabwe, Harare, Zimbabwe. The MINREST program is financially supported by the Directorate General for International Cooperation (DGIS), Ministry of Foreign Affairs of the Netherlands, via the Netherlands University Foundation for International Co-operation (NUFFIC). The Ph.D. research of H. A. Jelsma is funded by The Netherlands Organization for Scientific Research (NWO), via The Netherlands Organization for Scientific Research in the Tropics (WOTRO).

REFERENCES

Anhaeusser, C. R. 1973. The evolution of the early Precambrian crust of Southern Africa. *Phil. Trans. R. Soc. Lond.* **A273**, 359–388.

Anhaeusser, C. R., Mason, R., Viljoen, M. J. & Viljoen, R. P. 1969. Reappraisal of some aspects of Precambrian shield geology. *Bull. geol. Soc. Am.* **80**, 2175–2200.

Anhaeusser, C. R. & Viljoen, M. J. 1986. Archaean metallogeny of Southern Africa. In: *Mineral Deposits of Southern Africa, Vol. I* (edited by Anhaeusser, C. R. & Maske, S.). Geol. Soc. S. Africa, Johannesburg, 33–42.

Baldock, J. W. & Evans J. A. 1988. Constraints on the age of the Bulawayan Group metavolcanic sequences, Harare greenstone belt, Zimbabwe. *J. Afr. Earth Sci.* **7**, 795–804.

Bateman, R. 1984. On the role of diapirism in the segregation, ascent and final emplacement of granitoid magmas. *Techonophysics* **11**, 211–231.

Bleeker, W. & Westra, L. 1987. The evolution of the Mustio gneiss dome, Svecofennides of SW Finland. *Precambrian Res.* **36**, 227–240.

Brun, J. P., Gapais, D., Cogne, J. P., Ledru, P. & Vigneresse, J. L. 1990. The Flamanville Granite (Northwest France): an unequivocal example of a syntectonically expanding pluton. *Geol. J.* **25**, 271–286.

Brun, J. P., Gapais, D. & Le Theoff, B. 1981. The mantled gneiss domes of Kuopio (Finland): Interfering diapirs. *Tectonophysics* **74**, 283–304.

Brun, J. P. & Pons, J. 1981. Strain patterns of pluton emplacement in a crust undergoing non-coaxial deformation, Sierra Morena, Southern Spain. *J. Struct. Geol.* **3**, 219–229.

Coward, M. P. 1981. Diapirism and gravity tectonics: Report of a Tectonic Studies Group conference held at Leeds University, 25–26 March 1980. *J. Struct. Geol.* **3**, 89–95.

Cruden, A. R. 1988. Deformation around a rising diapir modelled by creeping flow past a sphere. *Tectonics* **7**, 1091–1101.

Cruden, A. R. 1990. Flow and fabric development during the diapiric rise of magma. *J. Geol.* **98**, 681–698.

De Wit, M. J. & Ashwall, L. D. 1986. Workshop on the tectonic evolution of greenstone belts. *LPI Technical Report* 86–10.

Dixon, J. M. 1975. Finite strain and progressive deformation in models of diapiric structures. *Tectonophysics* **28**, 89–24.

Dixon, J. M. & Summers, J. M. 1983. Patterns of total and incremental strain in subsiding troughs: Experimental centrifuged models of inter-diapir synclines. *Can. J. Earth Sci.* **20**, 1843–1861.

Dunnet, D. 1969. A technique of finite strain analysis using elliptical particles. *Tectonophysics* **7**, 117–136.

England, R. W. 1990. The identification of granitic diapirs. *J. geol. Soc. Lond.* **147**, 931–933.

Flinn, D. 1962. On folding during three dimensional progressive deformation. *Q. J. geol. Soc. Lond.* **118**, 385–428.

Gorman, B. E., Pearce, T. H. & Birkett, T. C. 1978. On the structure of Archaean Greenstone belts. *Precambrian Res.* **6**, 23–41.

Jelsma, H. A., Tomschi, H. P., Touret, J. L. R. & Kramers, J. D. 1990. Gold mineralisation at Shamva mine, northern Zimbabwe: An integrated structural–magmatic control. In: *Proc. Nuna Res. Conf. on Greenstone Gold and Crustal Evolution*, Val d'Or, Canada (Abs.), 58.

Lisle, R. J. 1977. Estimation of the tectonic strain ratio from the mean shape of deformed elliptical markers. *Geol. Mijnb.* **56**, 140–144.

Macgregor, A. M. 1951. Some milestones in the Precambrian of Southern Rhodesia. *Geol. Soc. S. Afr. Trans. & Proc.* **54**, 27–71.

Mareschal, J. C. & West, G. F. 1980. A model for Archean tectonism. Part 2. Numerical models of vertical tectonism in greenstone belts. *Can. J. Earth Sci.* **17**, 60–71.

Means, W. D. 1981. The concept of steady state foliation. *Tectonophysics* **78**, 179–199.

Means, W. D., Hobbs, B. E., Lister, G. S. & Williams, P. F. 1980. Vorticity and non-coaxiality in progressive deformations. *J. Struct. Geol.* **2**, 371–378.

Owens, W. H. 1984. The calculation of a best fit ellopsoid from elliptical sections on arbitrarily orientated planes. *J. Struct. Geol.* **6**, 571–578.

Paterson, S. R. & Tobisch, O. T. 1988. Using pluton ages to date regional deformations: Problems with commonly used criteria. *Geology* **16**, 1108–1111.

Paterson, S. R., Vernon, R. H. & Tobisch, O. T. 1989. A review of criteria for the identification of magmatic and tectonic foliation in granitoids. *J. Struct. Geol.* **11**, 349–364.

Platt, J. P. 1980. Archaean greenstone belts, a structural test of tectonic hypotheses. *Tectonophysics* **65**, 127–150.

Ramberg, H. 1981. *Gravity, Deformation and the Earth's Crust: Theory, Experiments and Geological Application* (2nd edn). Academic Press, London.

Ramsay, J. G. 1967. *Folding and Fracturing of Rocks*. McGraw-Hill, New York.

Ramsay, J. G. 1975. The structure of the Chindamora Batholith. *19th Ann. Rept. Res. Inst. African Geol. Univ. Leeds*, 81.

Ramsay, J. G. 1980. Shear zone geometry: a review. *J. Struct. Geol.* **2**, 83–99.

Ramsay, J. G. 1989. Emplacement kinematics of a granite diapir: the Chindamora batholith, Zimbabwe. *J. Struct. Geol.* **11**, 191–209.

Ramsay, J. G. & Huber, M. I. 1983. *The Techniques of Modern Structural Geology, Volume* 1: *Strain Analysis*: Academic Press, London.

Ramsay, J. G. & Woods, D. S. 1973. The geometric effects of volume change during deformation processes. *Tectonophysics* **16**, 263–277.

Ridley, J. R. & Kramers, J. D. 1990. The evolution and tectonic consequences of a tonalitic magma layer within Archean continents. *Can. J. Earth Sci.* **27**, 218–228.

Schmeling, H., Cruden, A. R. & Marquart, G. 1988. Finite deformation in and around a fluid sphere moving through a viscous medium: implications for diapiric ascent. *Tectonophysics* **149**, 17–34.

Schwerdtner, W. M., Stott, G. M. & Suttcliffe, R. H. 1983. Strain patterns of crescentic granitoid plutons in the Archaean greenstone terrain of Ontario. *J. Struct. Geol.* **5**, 419–430.

Schwerdtner, W. M., Suttcliffe, R. H. & Troëng, B. 1978. Patterns of total strain within the crestal region of immature diapirs. *Can. J. Earth Sci.* **15**, 1437–1447.

Schwerdtner, W. M. & Troëng, B. 1978. Strain distribution in arcuate diapiric ridges of silicone putty. *Tectonophysics* **50**, 13–28.

Shimamoto, T. & Ikeda, Y. 1976. A simple algebraic method for strain estimation from ellipsoidal objects; 1. Basic theory. *Tectonophysics* **36**, 315–317.

Snowden, P. A. 1984. Non-diapiric batholiths in the north of the Zimbabwe Shield. In: *Precambrian Tectonics Illustrated* (edited by Kröner, A. & Greiling, R.). Nägele und Obermiller, Stuttgart, 135–145.

Snowden, P. A. & Bickle, M. J. 1976. The Chinamora batholith: diapiric intrusion or interference fold? *J. geol. Soc. Lond.* **132**, 131–137.

Snowden, P. A. & Snowden, D. V. 1979. Geology of an Archaean batholith, the Chinamora batholith–Rhodesia. *Trans. geol. Soc. S. Afr.* **82**, 7–22.

Soula, J.-C. 1982. Characteristics and mode of emplacement of gneiss domes and plutonic domes in central-eastern Pyrenees. *J. Struct. Geol.* **4**, 313–342.

Stidolph, P. A. 1973. The granitic terrain north and east of the Shamva greenstone belt. *Spec. Pub. geol. Soc. S. Afr.* **3**, 121–125.

Stidolph, P. A. 1977. The geology of the country around Shamva. *Bull. geol. Surv. Rhodesia* **78**, 1–242.

Talbot, C. J. 1987. Strains and vorticity beneath a tabular batholith in the Zambesi belt, northeast Zimbabwe. *Tectonophysics* **138**, 121–158.

Talbot, C. J. & Jackson, M. P. A. 1987. Internal kinematics of salt diapirs. *Bull. Am. Ass. Petrol. Geol.* **71**, 185–202.

Taylor, P. N., Kramers, J. D., Moorbath, S., Wilson, J. F., Orpen, J. L. & Martin, A. 1991. Pb–Pb, Sm–Nd and Rb–Sr geochronology in the Archean craton of Zimbabwe. *Chem. Geol. (Isot. Geosci. Sect.)* **87**, 175–196.

Tobisch, O. T., Saleeby, J. B. & Fiske, R. S. 1986. Structural history of continental volcanic arc rocks, Eastern Sierra Nevada, California: a case for expansional tectonics. *Tectonics* **5**, 65–94.

Van Den Eeckhout, B., Grocott, J. & Vissers, R. 1986. On the role of diapirism in the segregation, ascent and final emplacement of granitoid magmas—discussion. *Tectonophysics* **127**, 161–169.

Veenhof, R. P. & Stel, H. 1991. A cleavage triple point and its mesoscopic structures: the Mustio Sink (Svecofennides of SW Finland). *Precambrian Res.* **50**, 269–282.

Viewing, K. A. & Harrison, N. M. 1973. A geological reconnaissance survey of the Chinamora batholith near Salisbury, Rhodesia. *Spec. Publ. geol. Soc. S. Afr.* **3**, 419–431.

Viljoen, M. A. & Viljoen, R. P. 1969. A reappraisal of the granite-greenstone terrains of shield areas based on the Barberton model. *Spec. Publ. geol. Soc. S. Afr.* **2**, 245–274.

Wilson, J. F. 1979. A preliminary reappraisal of the Rhodesian Basement Complex. *Spec. Publ. geol. Soc. S. Afr.* **5**, 1–123.

Wilson, J. F., Bickle, M. J., Hawkesworth, C. J., Martin, A., Nisbet, E. G. & Orpen, J. L. 1978. Granite–greenstone terrains of the Rhodesian Archaean craton. *Nature* **271**, 23–27.